RSC Advances

ROYAL SOCIETY OF CHEMISTRY

www.rsc.org/advances

RSC Advances

ARTICLE

Catalytic behaviour of TiO_2–ZrO_2 binary oxide synthesized by sol-gel process for glucose conversion to 5-hydroxymethylfurfural

Received 00th January 20xx,
Accepted 00th January 20xx

DOI: 10.1039/x0xx00000x

www.rsc.org/

Luqman Atanda,[a] Adib Silahua,[b] Swathi Mukundan,[a] Abhijit Shrotri,[c] Gilberto Torres-Torres[b] and Jorge Beltramini[a*]

The catalytic application of as-synthesized TiO_2–ZrO_2 binary oxides was examined for the conversion of glucose to produce 5-hydroxymethylfurfural (HMF). Highest HMF yield (74%) at glucose concentration of 5 wt% was obtained with TiO_2–ZrO_2 (1/1) and Amberlyst 70 catalyst system in a water-THF biphasic reaction system. Notably, a much higher HMF yield (86%) was achieved when the organic phase of the biphasic system was replaced with dioxane. The increased product yield may be ascribed to the role of dioxane as an aqueous phase modifier that stabilizes HMF in the reactive phase as well as promotes partitioning of HMF into the extractive layer. Furthermore, the combined catalyst and biphasic solvent systems were also effective for the conversion of glucose polymers to HMF.

1. Introduction

Diversification of energy sources to reduce dependence on fossil fuels has motivated a strong research interest to attain sustainability in biomass conversion to transportation fuels and chemical building blocks.[1-6] For example, 5-hydroxymethylfurfural (HMF), which is a dehydration product of biomass-derived carbohydrates, has been identified as a versatile intermediate for value-added chemicals and biofuels.[7, 8] Conventionally, HMF is produced by triple dehydration of hexoses in an acidic medium.[9] Throughout these studies, it is generally accepted that glucose is less reactive than fructose because of its stable glucopyranose structure.[10, 11] However, glucose is a preferred starting material since it is cheaper and relatively available in abundance.[12, 13] Significant improvement on glucose conversion to HMF can be attained by performing the reaction in the presence of a metal halide, which catalyzes the isomerization of glucose to fructose, in tandem with mineral acids[14, 15] or acidic ionic liquid.[16-19] In spite of these recent achievements, efficient isolation and purification of HMF from the reaction medium remains a challenge.[20] On the other hand, heterogeneous catalysis is a promising cost-effective route for large scale HMF synthesis due to ease of catalyst handling, simple separation and recovery steps.

Several metal oxides, such as titania (TiO_2) and zirconia (ZrO_2) have been reported to possess exceptional redox and acid-base properties, which makes them a good choice as catalysts and catalyst supports.[21] Moreover, catalytic property of these oxides can be improved by mixing them together. This improvement is attributable to the generation of new catalytic sites due to strong interaction between the individual oxides, giving rise to a mixed metal oxide of profound surface acid-base properties and high thermal stability.[21] Thus, the superior properties of TiO_2–ZrO_2 binary oxide make it more suitable for catalytic applications than individual component oxide.[22-25] However, limited reports exist on the catalytic potential of TiO_2–ZrO_2 binary oxide to transform biomass-derived carbohydrates to HMF. Chareonlimkun and co workers[26] explored simultaneous hydrolysis/dehydration of a variety of lignocellulosic biomass under hot compressed water. They found that superior product yield was achieved with TiO_2–ZrO_2 binary oxide in comparison with TiO_2 and ZrO_2, which was ascribed to the synergy between the base sites of ZrO_2 and acid sites of TiO_2. Furthermore, catalyst preparation technique and calcination temperature were two parameters observed to influence the acid-base properties of the oxides, hence their catalytic reactivity.

In this study, we prepared a series of TiO_2–ZrO_2 binary oxides by a neutral amine sol-gel technique. The effect of TiO_2/ZrO_2 weight ratio on the acid-base properties of the binary oxides was examined by temperature programmed desorption of NH_3 and CO_2. Furthermore, the pyhsico-chemical properties of the oxide materials were investigated with N_2 adsorption-desorption, XRD, Raman and XPS techniques. We evaluated their catalytic performance in transforming glucose to HMF using water as the reaction solvent. In addition, the cooperative role of a co-solvent and a solid Bronsted acid co-catalyst was examined. Thereafter, the robustness of the

[a] Nanomaterials Centre, Australian Institute for Bioengineering & Nanotechnology and School of Chemical Engineering, The University of Queensland, Brisbane, St. Lucia 4072, Australia. E-mail: j.beltramini@uq.edu.au
[b] Heterogeneous Catalysis Laboratory, Universidad Juárez Autónoma de Tabasco, Cunduacán, Tabasco, México.
[c] Catalysis Research Center, Hokkaido University, Saporro, Japan.
† Electronic Supplementary Information (ESI) available: supplemented data. See DOI: 10.1039/x0xx00000x

reaction system was extended to other sugar substrates such as cellobiose, sucrose and cellulose.

2. Experimental

2.1. Chemicals and materials

Glucose, fructose, sucrose, cellobiose, cellulose, 5-hydroxymethylfurfural (HMF), levoglucosan, titanium IV butoxide, zirconium IV butoxide, ammonium hydroxide solution (28 wt%), phosphotungstic acid ($H_3PW_{12}O_4$), silicotungstic acid ($H_4SiW_{12}O_4$), propan-1-ol, butan-1-ol, Methyl isobutyl ketone (MIBK) and Nafion NR50 were obtained from Sigma-Aldrich. Tetrahydrofuran and 1,4-dioxane were obtained from Merck Millipore. Amberlyst 70 was supplied by Roms and Haas. All the chemicals were used without further purification. Ultrapure water (18.2 MΩ cm^{-1}) from Elga distillation system was used for all the experiment.

2.2. Preparation of TiO_2–ZrO_2 binary oxides

TiO_2, ZrO_2 and a series of TiO_2–ZrO_2 with varying weight percentage of TiO_2 to ZrO_2 were prepared by sol-gel method. The sol was prepared by the dropwise addition of the alkoxide precursors into an aqueous solution containing butan-1-ol under stirring. The pH of the solution was adjusted to 7 by adding ammonium hydroxide solution and the resulting solution was maintained at 70 °C under reflux for 24 h. After gelation, excess solvent was removed using rotary evaporator and followed by vacuum drying at 120 °C for 12 h. The dried samples were then calcined at 500 °C for 12 h to obtain the corresponding pure or mixed oxides.

2.3. Preparation of heteropolyacid salts - $Cs_{2.5}PW$ and $Cs_{3.5}SiW$

Cesium salt of $H_3PW_{12}O_4$ and $H_4SiW_{12}O_4$ were obtained by titrating an aqueous solution of $H_3PW_{12}O_4$ or $H_4SiW_{12}O_4$ (0.08 M) with an aqueous solution of Cs_2CO_3 (0.25 M) while stirring. The resulting precipitate was dried at 110 °C for 12 h in vacuum and then calcined at 300 °C for 3 h.

2.4. Catalyst characterization

Powder XRD measurements were performed on a Rigaku Miniflex with a monochromatic CoKα radiation (30 kV, 15 mA) in the 2ϑ range 10–90 °. Nitrogen adsorption data were collected using a Micromeritics TriStar II 3020 surface area and porosity analyzer. Prior to physisorption measurements, all samples were outgassed under vacuum at 200 °C overnight. The specific surface area of the oxides was determined applying the BET method. Total pore volumes were estimated from the amount of adsorbed N_2 at p/p_o value of 0.99. Temperature programmed desorption (TPD) of ammonia and CO_2 were performed on a BEL Japan BELCAT-A instrument equipped with a mass spectrometer and thermal conductivity detector (TCD). This was used to determine the amount and strength of the acid-base sites available on the catalyst samples. About 70 mg of sample was saturated with either NH_3 or CO_2 as the probe gas at 100 °C, flushed with He to remove physisorbed gas and then ramped to 800 °C at a heating rate of 10 °C/min under He flow. Pyridine infrared spectroscopy was used to determine the nature of surface acid sites. Pyridine was chemisorbed on the catalyst surface (50 mg) at 150 °C. Excess gaseous and physisorbed pyridine were removed by holding the temperature at 150 °C for 30 min under N_2 flow. FTIR spectra were collected using a Nicolet 6700 (Smart Orbit Accessory) at 128 scans and 4 cm^{-1} resolution. X-ray photoelectron spectra (XPS) of the catalysts was acquired using Kratos Axis ULTRA X-ray photoelectron spectrometer equipped with a 165 mm hemispherical electron energy analyser using a monochromatic Al Kα (1486.6 eV) x-ray source. The binding energies were referenced to C 1s peak at 284.8 eV. Raman spectroscopy was performed on a Reinshaw In-Via Raman microscope equipped with a Leica DM LM Microscope using a 633 nm HPNIR diode laser as an excitation source. The raman spectra were collected with a CCD array detector in the region of 100–2000 cm^{-1} at 4 cm^{-1} resolution and acquisition time of 1 s.

2.5. Catalytic activity procedure and product analysis

Glucose conversion to HMF was carried out in a Parr reactor. In a typical experimental run, required amount of glucose, solvent and catalysts were charged into a 300 mL reactor, purged with high purity Ar and then pressurized to 30 bar. The reactor was ramped to its set point temperature which was monitored by a thermocouple inside a thermowell immersed in the reaction mixture. Time zero of the reaction was defined as the time when the reactor reached its set point temperature usually after approx. 9 mins of ramping. Catalytic runs were repeated for data reproducibility. Experimental errors were in the range of ±2%. Liquid samples were taken after reaction and the concentration of the product species were quantified using Shimadzu Prominence HPLC with a Bio-Rad Aminex HPX-87H as the analytical column and both RID–10 (refractive index) and SPD–M20A (UV–Vis) as detectors. The HPLC was operated under the following conditions: oven temperature, 50 °C, mobile phase, 5 mM H2SO4; flow rate, 0.6 ml/min; injection volume, 20 µL. The concentrations of glucose, fructose, HMF and other identifiable products were quantified by HPLC analysis through the external standard method and calibration curves of commercially available standard substrates. Glucose conversion (Conv. mol %) and products yield (mol %) were calculated according to:

$$Conv.(mol\%) = \left(1 - \frac{nC_6}{nC_6^o}\right) \times 100\%$$

$$\text{Product yield}\,(mol\%) = \left(\frac{n_i}{nC_6^o}\right) \times 100\%$$

where nC_6 and nC_6^o denote number of moles of C_6 sugar in the product and feed, respectively, and n_i is the number of moles of identified products (HMF, levulinic acid, levoglucosan etc.).

3. Results and discussion

3.1. Characterization of TiO_2–ZrO_2 binary oxides

The crystalline phases of TiO_2, ZrO_2, and TiO_2–ZrO_2 binary oxides were investigated using XRD analysis. The XRD pattern of the oxides is shown in Fig. 1.

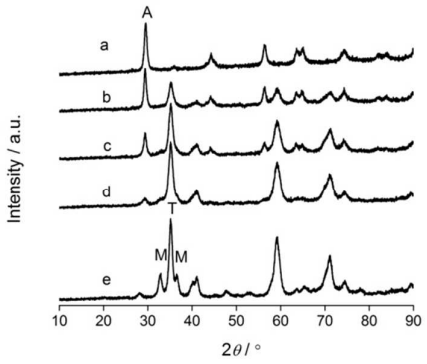

Fig. 1 XRD patterns of: a) TiO_2, b) TiO_2–ZrO_2 (3/1), c) TiO_2–ZrO_2 (1/1), d) TiO_2–ZrO_2 (1/3) and e) ZrO_2. A: anatase; M: monoclinic; T: tetragonal

The indexed diffraction pattern of TiO_2 revealed that it exists as anatase phase, whereas for ZrO_2, a combination of monoclinic (*m*-ZrO_2) and tetragonal (*t*-ZrO_2) phases were identified, corresponding to 2ϑ values of 28.1 ° and 35.1 °, respectively. However, in the case of the binary oxides, regardless of the TiO_2/ZrO_2 ratio, Fig. 1b-d show a composite diffraction pattern that corresponds to the anatase-TiO_2 (2ϑ = 29.5 °) and *t*-ZrO_2 (2ϑ = 35.1 °) phases. The *m*-ZrO_2 phase ceases to exist even with the smallest TiO_2/ZrO_2 ratio i.e. 1:3. This indicates that *t*-ZrO_2 phase was stabilized due to the presence of Ti atom in ZrO_2 lattice, which results in dissimilar grain boundaries that prevents the formation and crystal growth of the monoclinic phase.[27] Moreover, no diffraction peaks related to zirconium titanate phase could be detected. It may be that this phase is composed of very small particles below detection limit or could exist in an amorphous state. Surface area and pore volume as determined by N_2-adsorption measurement are summarized in Table 1. The surface areas of TiO_2 and ZrO_2 are 79.4 m^2/g and 40.8 m^2/g, respectively. ZrO_2 has the lowest surface area of all the oxides. Surface areas of the binary oxides gradually increase as it becomes enriched with TiO_2.

Table 1 Textural and acid-base properties of the mixed oxides

Catalyst	S_{BET}[a] (m^2/g)	Pore vol[b] (cc/g)	Acid site conc.[c] (μmol/g)	Basic site conc.[d] (μmol/g)
TiO_2	79.4	0.33	476.6	12.1
TiO_2-ZrO_2 (3/1)	68.0	0.27	469.8	16.7
TiO_2-ZrO_2 (1/1)	62.0	0.18	452.3	23.7
TiO_2-ZrO_2 (1/3)	60.0	0.13	372.2	27.5
ZrO_2	40.8	0.12	202.1	34.2

[a] Specific surface area calculated by the BET method. [b] Pore vol calculated at P/P_o = 0.99. [c] Calculated from ammonia–TPD. [d] Calculated from CO_2–TPD

Table 1 also reports the acid–base property of the oxides measured by temperature programme desorption (TPD). From the table it can be seen that as the ZrO_2 content increases, acidity of the oxides reduces with a corresponding increment in basicity. Furthermore, the distribution and strength of the acid and base sites is shown in Fig. S1. Acid[28] and base[29] strength is categorized as low, medium and strong, depending on desorption temperature. The CO_2–TPD profile of ZrO_2 (Fig. S1a) shows three peaks centered at 185 °C, 550 °C and 610 °C, which can be attributed to weak and strong basic sites, respectively. Meanwhile, TiO_2 is predominantly characterized with a small broad peak centered at 600 °C corresponding to strong basic site. TiO_2–ZrO_2 (1/1) has a CO_2 desorption profile defined by two well resolved peak signals centered at 170 °C and 550 °C, similar to that of ZrO_2. On the other hand, ammonia desorption profile of the oxides is shown in Fig. S1b. TiO_2 shows a large concentration of weak-to-medium strength acid sites, whereas ZrO_2 is characterized by strong acid sites albeit weak concentration. TiO_2–ZrO_2 (1/1) shows a composite profile of high concentration of weak-to-medium acid sites and low concentration of strong acid sites. The nature of the acid sites available on the oxides was identified through infrared spectra of adsorbed pyridine. As shown in Fig. 2, the peak intensities observed indicates the oxides are characterized by Lewis acid sites. Pure TiO_2 displays intense bands at 1446 cm^{-1} and 1608 cm^{-1} with moderate bands at 1489 cm^{-1} and 1575 cm^{-1}.

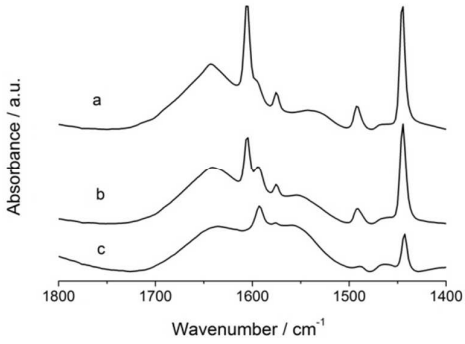

Fig. 2 Infrared spectra of pyridine adsorbed on: a) TiO_2, b) TiO_2–ZrO_2 (1/1) and c) ZrO_2

Meanwhile, pure ZrO_2 showed fewer and less intense bands, which agrees well with NH_3–TPD result that ZrO_2 has fewer acid sites than TiO_2. TiO_2–ZrO_2 (1/1) mixed oxide has peak reflections similar to TiO_2, though with slightly reduced intensity. Moreover, it has an extra peak at 1590 cm^{-1}, which is a reflection of ZrO_2.

Surface analysis of the oxides was examined by Raman and XPS. Raman spectra of all the oxides are shown in Fig. 3. Fig. 3a depicts Raman spectrum of TiO_2 is dominated by vibrational bands at 144, 400, 515 and 635 cm^{-1}, which can be attributed to $v_1(E_g)$, $v_2(B_{1g})$, $v_3(A_{1g})$ or $v_3(B_{1g})$ and $v_4(E_g)$, respectively, of anatase-TiO_2 phase.[30] $v_1(E_g)$ and $v_2(B_{1g})$ represent the O–Ti–O

bending vibrational mode, whereas $v_3(A_{1g})$ or $v_3(B_{1g})$ and $v_4(E_g)$ represent the Ti–O bond stretching vibrational mode.[31]

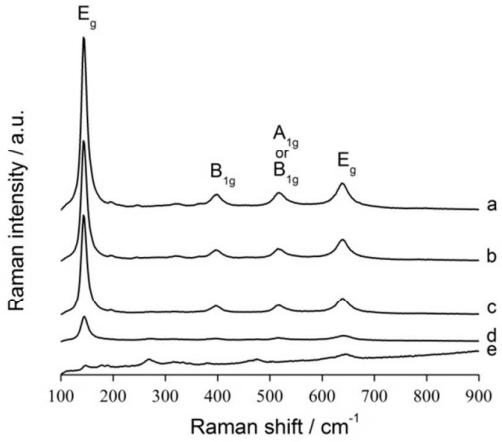

Fig. 3 Raman spectra of: a) TiO_2, b) TiO_2–ZrO_2 (3/1), c) TiO_2–ZrO_2 (1/1), d) TiO_2–ZrO_2 (1/3) and e) ZrO_2

Fig. 3b through 3d shows that the intensity of these bands attenuates gradually as the binary oxide becomes enriched with ZrO_2. Elemental surface compositions and binding energies from the XPS analysis are listed in Table 2. The changes in the surface composition of Ti and Zr atoms are consistent with the observed pattern in the Raman intensities of the oxides, wherein elemental composition of Ti declines as ZrO_2 content is increased. This indicates mutual interaction between the oxides as a result of Ti^{4+} substitution with Zr^{4+} and vice versa, which is also accompanied by structural changes as depicted by the variations in the Raman signals of the metal oxides.

Table 2 Binding energies and surface composition of TiO_2–ZrO_2 mixed oxides from XPS

Sample	Surface atoms (%)				BE (eV)		
	Ti	Zr	C	O/(Ti+Zr)	O 1s	Ti $2p_{3/2}$	Zr $3d_{5/2}$
TiO_2	20.3	-	33.4	2.28	529.9	458.6	-
TiO_2 - ZrO_2 (3/1)	17.8	3.3	32.2	2.21	529.9	458.6	182.0
TiO_2 - ZrO_2 (1/1)	13.0	7.5	34.5	2.20	529.9	458.6	182.1
TiO_2 - ZrO_2 (1/3)	7.1	15.5	29.6	2.12	529.9	458.6	182.2
ZrO_2	-	22.3	29.0	2.18	529.8	-	182.2

Significant carbon atom was also identified on all the oxides. This carbon impurity may be understood to come from the alkoxy groups originating from the sol-gel process. The binding energies associated with Ti $2p_{3/2}$, Zr $3d_{5/2}$ and O 1s are also reported in Table 2. Binding energies of 458.6 eV and 182.2 eV corresponds to Ti $2p_{3/2}$ and Zr $3d_{5/2}$ of TiO_2 and ZrO_2 single oxide, respectively. O 1s peak of TiO_2 and ZrO_2 are assigned 529.9 eV and 529.8 eV binding energies, respectively. These values confirm that both Ti and Zr exist in the tetravalent oxidation state.[32] As for the binary oxides, Ti $2p_{3/2}$ has similar binding energy as that of pure TiO_2 while Zr $3d_{5/2}$ is about 0.1–0.2 eV lower than that of pure ZrO_2. This shift towards lower binding energy may indicate the substitution of some Zr^{4+} ions with Ti^{4+}, thereby causing reduction of interatomic potentials due to reduced overall atomic size.[33]

3.2. Activity tests

Catalytic application of the metal oxide system was examined for the conversion of biomass-derived sugars into HMF, using glucose as a model compound. Initial reactivity study conducted with water as the reaction medium was used to evaluate catalytic performance of the oxides. Dependence of glucose conversion capacity and products yield in relation to the composition of TiO_2/ZrO_2 binary oxide is shown in Fig. 4. It can be seen from the Figure that glucose conversion ranges from 72–86%, with HMF as the main product. With increase in ZrO_2 content of the binary oxide, glucose conversion decreases whereas yield of HMF increases and goes through a maximum at TiO_2/ZrO_2 (1:1) followed by a minor decline.

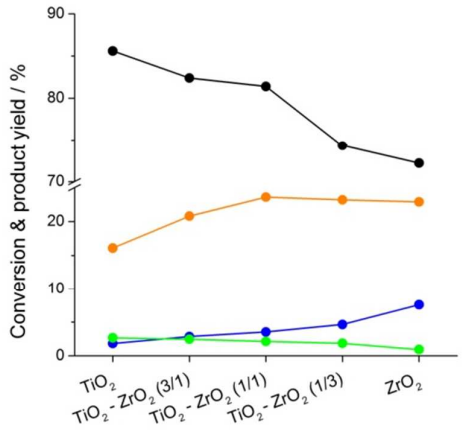

Fig. 4 Glucose conversion to HMF over TiO_2–ZrO_2 binary oxides in an aqueous medium. Reaction conditions: 2 g glucose, 0.8 g catalyst wt., 3 h reaction time, 175 °C reaction temperature, 100 ml water. (●), glucose conversion and product yields: (●) fructose, (●) HMF, (●) levulinic acid.

This occurrence may be interpreted in relation to the acidity of the binary oxides. TiO_2 possesses large concentration of acid sites that can dehydrate fructose, an initial product of glucose isomerization, into HMF. Hence, least concentration of fructose is observed on TiO_2 but the value rises gradually with declining acidity of the binary oxide due to increase in ZrO_2 content. More so, in an aqueous acidic medium, HMF rehydrates to give levulinic acid and may also react with

glucose or other reactive intermediates to form humins. Therefore, as TiO_2 content of the binary oxide increases, which correlates to increasing acidity, there is an upward trend of both the yield of levulinic acid and glucose conversion as shown in Fig. 5. To support this hypothesis, another reaction was conducted at 160 °C for 5 h with fructose as feed but keeping other reaction conditions same. As shown in Table S1, fructose conversion of 95.3% and 85.6% was attained on TiO_2 and ZrO_2, respectively. Even though fructose conversion on TiO_2 was superior, a better yield of HMF was achieved on ZrO_2 (29.6 vs 24.1%). Regardless of the pure metal oxide, it is noteworthy that fructose conversion to HMF occurred relatively faster in comparison to glucose. This indicates that glucose proceeds via fructose to produce HMF. From Fig. 4, an optimum HMF yield of 23.6% is obtained with TiO_2–ZrO_2 (1/1), which can be ascribed to modified acid–base properties of the binary oxide. The mutual interaction of the pure oxides provided a moderate acid–base concentration (Table 1) suitable for the glucose-to-HMF reaction. This cooperative interaction between the acid–base sites on TiO_2–ZrO_2 has been reported in literature, wherein glucose is isomerized to fructose preferentially on the basic sites of ZrO_2 and subsequent dehydration of fructose to HMF on the acid sites of TiO_2.[26, 34, 35]

Next, we examined the role of reaction medium on the formation rate of HMF. A water-lean medium was considered since the yield of HMF in a single aqueous medium is relatively low. Tetrahydrofuran (THF) was chosen as a co-solvent. It lacks hydroxyl groups and has the potential to suppress side reactions.[36] In spite of adding THF to water in a ratio of 4:1 (v/v) to make up the reaction medium, glucose conversion and yield of HMF were not significantly enhanced as shown in Fig. S2. Contrarily, a remarkable increment of HMF yield by almost 3 fold from 23.6% to 71% was observed after the introduction of NaCl (20 wt% of the aqueous phase) into the THF/water solvent mix. The addition of NaCl promoted solvent partitioning into two phases: a reactive aqueous phase and an extractive organic phase. This allowed in situ extraction of HMF from the aqueous phase into the organic phase, thereby preventing undesired side reactions. Moreover, the continuous extraction shifts the reaction equilibrium to produce more HMF. Furthermore, we investigate the role of solid Bronsted acid supports such as Amberlyst 70, Nafion NR50, $Cs_{2.5}PW$ and $Cs_{3.5}SiW$ as co-catalysts, as it has been observed that co-existence of Lewis and Bronsted bifunctional acidity promote glucose conversion to HMF.[37, 38] Herein, co-catalysts refer to physical mixture of TiO_2–ZrO_2 (1/1) and the solid Bronsted acid supports. Under comparable reaction conditions, Fig. 5 clearly demonstrates that the choice of Amberlyst 70 as co-catalyst is the most beneficial, resulting in HMF yield of about 85.6 % at a near-complete glucose conversion. Meanwhile, using the solid Bronsted acid supports without the binary oxide gave lesser HMF yields. For instance, approximately 10% yield HMF was achieved with $Cs_{3.5}SiW$ at complete glucose conversion. This indicates that the dominant route for glucose conversion to HMF is via intermediate fructose formation, which is otherwise promoted by Lewis acid or base isomerisation of glucose.

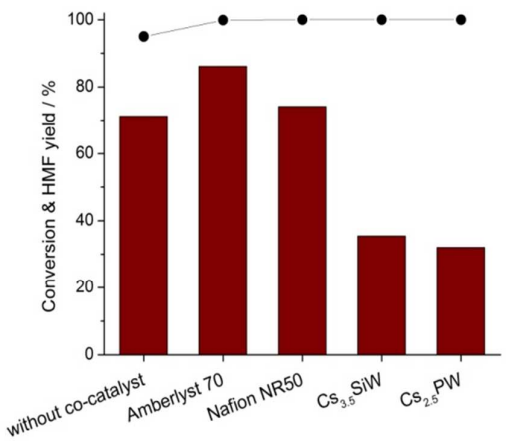

Fig. 5 Catalytic conversion of glucose over TiO_2–ZrO_2 with solid acid co-catalysts. Reaction conditions: 2 g glucose, 0.8 g catalyst wt. (TiO_2–ZrO_2(1/1)/co-catalyst ratio = 1/1 w/w), 100 ml solvent (THF/water = 4/1 v/v), 4 g NaCl, 3 h reaction time, 175 °C reaction temperature.

HMF yield varies with the co-catalysts as follows: Amberlyst 70 (85.6%) > Nafion NR50 (73.4%) > $Cs_{3.5}SiW$ (35.2%) > $Cs_{2.5}PW$ (31.8%). The observed variation can be related to the acid strength of the co-catalysts. $H_3PW_{12}O_{40}$ and $H_4SiW_{12}O_{40}$ are superacids of very strong acid strength (H_0 = –13.6).[39] Nevertheless, $H_3PW_{12}O_{40}$ is slightly more acidic than $H_4SiW_{12}O_{40}$.[40] $Cs_{2.5}PW$ has acid strength similar to the parent phosphotungstic acid[41] and correspondingly, $Cs_{3.5}SiW$ is anticipated to possesses weaker acid strength compared to $Cs_{2.5}PW$. Hammett acidity function, H_0, of Nafion NR50 is –12,[42] whereas Amberlyst 70 has a similar measure of acidity as Amberlyst 35 with a H_0 value of –5.6.[43] From the H_0 values, Amberlyst 70 possesses the lowest Bronsted acidity. We may infer that there is a linear correlation between Bronsted acid strength and yield of HMF. The stronger the Bronsted acidity, the greater the propensity of HMF to degrade to huminic compounds because of the strong affinity of HMF onto the Bronsted acid sites.[44, 45] For this reason, the pair of TiO_2–ZrO_2 (1/1) and Amberlyst 70 appears to be the optimum catalytic system for the transformation of glucose to HMF. Effectiveness of the catalytic system was further evaluated for HMF synthesis at a higher initial glucose concentration. As shown in Fig. S6, we observed a reduction in HMF yield as the initial glucose concentration was increased from 2 to 5 wt%, which can be ascribed to polymerization and cross-polymerization of HMF to humins.[46-48] Visually, we observed fine dark-brown powder deposit on the reactor wall, which was more prominent at high glucose concentration. We speculate that the choice of organic solvent of the biphasic system may help reduce the severity of humin compounds formation. Hence, we decided to replace THF with other organic solvents such as

1-butanol, 1-propanol, methyl-isobutyl-ketone (MIBK) and 1,4-dioxane. As shown in Fig. 6, dioxane was the most effective, selectively producing approximately 86% yield of HMF.

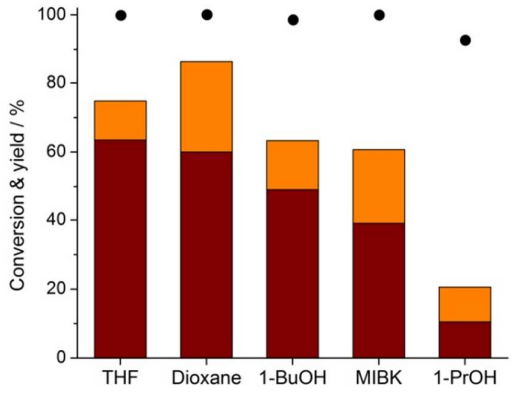

Fig. 6 Influence of organic solvent in the biphase system on selective HMF yield with TiO_2–ZrO_2 (1/1) and Amberlyst 70 catalysts. Reaction conditions: 5 g glucose, 2 g catalyst weight (TiO_2-ZrO_2/Amberlyst = 1/1 w/w), 100 ml solvent (THF/water = 4/1 v/v), 4 g NaCl, 3 h reaction time, 175 °C reaction temperature. (●) Glucose conversion, (■) HMF_{org} and (■) HMF_{aq}.

Not only does dioxane enables good partitioning of HMF into the organic phase, but HMF concentration in the reactive aqueous phase is also highest, suggesting HMF is more stable in the water-dioxane biphase system. Although the cause of this phenomenon is unclear, we consider that the reactive phase was modified by dioxane thereby minimizing degradation of HMF into humins. The outcome of HMF production using water-dioxane biphasic reaction system is promising and provides a step further towards achieving an efficient reaction medium for scaling-up. But dioxane poses a degree of health risk due to its carcinogenic activity,[49] which must be taken into consideration. More so, replacing homogeneous catalysts with solid ones facilitate product separation and solvent recovery, which further improves the attractiveness of biphasic system for industrial application. For instance, we contrasted the catalytic performance of our catalyst system with those reported in literature. Gallo et al.[36] reported HMF yields of 59%, 55% and 63% using a combination of Amberlyst 70 and Sn-Beta with γ-valerolactone, γ-hexalactone and tetrahydrofuran, respectively, as organic solvents of a water-organic biphasic system. Yang et al.[50] demonstrated the conversion of glucose with $AlCl_3$ and HCl using THF as a co-solvent with water to give up to 62% HMF yield. Yang et al.[51] reported 53% yield of HMF using a combination of Sn-Beta and HCl to catalyze glucose dehydration in water with THF as extracting solvent.

Lastly, the catalytic system of TiO_2–ZrO_2 mixed oxide and Amberlyst 70 was examined for the synthesis of HMF using cellobiose, sucrose and cellulose. The result of HMF synthesis from these various sugar substrates is given in Table 3.

Table 3 Catalytic transformation of sugars to HMF[a]

Entry	Substrate	Temp. °C	Conversion (%)	HMF yield (%)
1	Glucose	175	99.9	85.9
2	Sucrose	180	>99	86.5
3	Cellobiose	180	>99	80.8
4	Cellulose	180	42.1	25.5

[a] Reaction conditions: 2 g substrate, solvent volume 100 mL (THF/water = 4/1), 0.8 g catalyst wt. (TiO_2–ZrO_2/Amberlyst 70 = 1), 3 h reaction time, 30 bar Ar pressure.

As observed in Table 3, HMF yield from cellobiose and sucrose is above 80%, nevertheless, sucrose gave a better yield. This is because sucrose is a dimer of glucose-fructose molecules, which makes it more reactive than cellobiose, a dimer of glucose-glucose molecules. As anticipated, cellulose was found to be the least reactive with HMF yield of 25.5%. This is attributable to the strong intermolecular hydrogen bonding of cellulose. A higher temperature such as 200 °C or greater is required for reactivity of cellulose to improve due to increased hydrothermolysis.[52] However, Amberlyst 70 has relatively poor thermal stability at such high temperature, thereby restricting its usage to typically 190 °C.[53]

4. Conclusions

We demonstrated that TiO_2–ZrO_2 (1/1) binary oxide is an effective catalyst for the production of HMF from glucose. A water–THF biphasic system remarkably enhanced HMF formation rate. Furthermore, co-addition of Amberlyst 70 to the reaction system selectively improved the formation of HMF. We also show that at relatively high glucose loading (5 wt%), good yield of HMF is achievable. This was further improved by replacing the organic solvent of the biphase system with dioxane, due to its added advantage of modifying the aqueous phase to minimize degradation of HMF to humins. HMF was also obtained in high yields via the transformation of cellobiose and sucrose. Meanwhile, direct conversion of cellulose to HMF was more difficult due to its poor reactivity. Lastly, we conclude that a single multi-functional solid catalytic system and an organic solvent of high partitioning coefficient that can also serve as a phase modifier advance the realization of biphasic reaction system for large scale HMF synthesis.

Acknowledgements

The authors gratefully acknowledge the funding from the Sugar Research Australia (SRA) and ARC Centre of Excellence for Functional Nanomaterials at The University of Queensland, Australia. We also acknowledge the facilities and the scientific and technical assistance of the Australian Microscopy &

Microanalysis Research Facility at The University of Queensland.

Notes and references

1 G. W. Huber, S. Iborra and A. Corma, *Chem. Rev.*, 2006, **106**, 4044-4098.
2 G. W. Huber and A. Corma, *Angew. Chem. Int. Ed.*, 2007, **46**, 7184-7201.
3 J. N. Chheda, G. W. Huber and J. A. Dumesic, *Angew. Chem. Int. Ed.*, 2007, **46**, 7164-7183.
4 F. Cherubini, *Energy Convers. Manage.*, 2010, **51**, 1412-1421.
5 J. C. Serrano-Ruiz, R. Luque and A. Sepulveda-Escribano, *Chem. Soc. Rev.*, 2011, **40**, 5266-5281.
6 R. A. Sheldon, *Green Chem.*, 2014, **16**, 950-963.
7 J. J. Bozell and G. R. Petersen, *Green Chem.*, 2010, **12**, 539-554.
8 Y. Román-Leshkov, C. J. Barrett, Z. Y. Liu and J. A. Dumesic, *Nature*, 2007, **447**, 982-985.
9 R.-J. van Putten, J. C. van der Waal, E. de Jong, C. B. Rasrendra, H. J. Heeres and J. G. de Vries, *Chem. Rev.*, 2013, **113**, 1499-1597.
10 J. N. Chheda, Y. Roman-Leshkov and J. A. Dumesic, *Green Chem.*, 2007, **9**, 342-350.
11 A. Osatiashtiani, A. F. Lee, D. R. Brown, J. A. Melero, G. Morales and K. Wilson, *Catal. Sci. Technol.* 2014, **4**, 333-342.
12 F. W. Lichtenthaler, *Acc. Chem. Res.*, 2002, **35**, 728-737.
13 A. I. Torres, P. Daoutidis and M. Tsapatsis, *Energy Environ. Sci.*, 2010, **3**, 1560-1572.
14 Y. J. Pagán-Torres, T. Wang, J. M. R. Gallo, B. H. Shanks and J. A. Dumesic, *ACS Catal.*, 2012, **2**, 930-934.
15 V. Choudhary, S. H. Mushrif, C. Ho, A. Anderko, V. Nikolakis, N. S. Marinkovic, A. I. Frenkel, S. I. Sandler and D. G. Vlachos, *J. Am. Chem. Soc.*, 2013, **135**, 3997-4006.
16 H. Zhao, J. E. Holladay, H. Brown and Z. C. Zhang, *Science*, 2007, **316**, 1597-1600.
17 G. Yong, Y. Zhang and J. Y. Ying, *Angew. Chem. Int. Ed.*, 2008, **47**, 9345-9348.
18 J. B. Binder and R. T. Raines, *J. Am. Chem. Soc.*, 2009, **131**, 1979-1985.
19 M. E. Zakrzewska, E. Bogel-Łukasik and R. Bogel-Łukasik, *Chem. Rev.*, 2011, **111**, 397-417.
20 S. P. Teong, G. Yi and Y. Zhang, *Green Chem.*, 2014, **16**, 2015-2026.
21 B. M. Reddy and A. Khan, *Catal. Rev.*, 2005, **47**, 257-296.
22 A. Kitiyanan, S. Ngamsinlapasathian, S. Pavasupree and S. Yoshikawa, *J. Solid State Chem.*, 2005, **178**, 1044-1048.
23 W. Zhou, K. Liu, H. Fu, K. Pan, L. Zhang, L. Wang and C.-c. Sun, *Nanotechnology*, 2008, **19**, 035610.
24 J.-Y. Kim, C.-S. Kim, H.-K. Chang and T.-O. Kim, *Adv. Powder Technol.*, 2010, **21**, 141-144.
25 K.-T. Li, I. Wang and J.-C. Wu, *Catal. Surv. Asia*, 2012, **16**, 240-248.
26 A. Chareonlimkun, V. Champreda, A. Shotipruk and N. Laosiripojana, *Bioresour. Technol.*, 2010, **101**, 4179-4186.
27 X. Fu, L. A. Clark, Q. Yang and M. A. Anderson, *Environ. Sci. Technol.*, 1996, **30**, 647-653.
28 M. Paul, N. Pal, P. R. Rajamohanan, B. S. Rana, A. K. Sinha and A. Bhaumik, *Phys. Chem. Chem. Phys.*, 2010, **12**, 9389-9394.
29 G. V. Sagar, P. V. R. Rao, C. S. Srikanth and K. V. Chary, *J. Phys. Chem. B*, 2006, **110**, 13881-13888.
30 W. F. Zhang, Y. L. He, M. S. Zhang, Z. Yin and Q. Chen, *J Phys D Appl Phys*, 2000, **33**, 912-916.
31 T. Ohsaka, F. Izumi and Y. Fujiki, *J. Raman Spectrosc.*, 1978, **7**, 321-324.
32 S. Polisetti, P. A. Deshpande and G. Madras, *Ind. Eng. Chem. Res.*, 2011, **50**, 12915-12924.
33 H.-R. Chen, J.-L. Shi, W.-H. Zhang, M.-L. Ruan and D.-S. Yan, *Chem. Mater.*, 2001, **13**, 1035-1040.
34 M. Watanabe, Y. Aizawa, T. Iida, R. Nishimura and H. Inomata, *Appl. Catal. A*, 2005, **295**, 150-156.
35 M. Watanabe, Y. Aizawa, T. Iida, T. M. Aida, C. Levy, K. Sue and H. Inomata, *Carbohydr. Res.*, 2005, **340**, 1925-1930.
36 J. M. R. Gallo, D. M. Alonso, M. A. Mellmer and J. A. Dumesic, *Green Chem.*, 2013, **15**, 85-90
37 E. Nikolla, Y. Román-Leshkov, M. Moliner and M. E. Davis, *ACS Catal.*, 2011, **1**, 408-410.
38 L. Atanda, S. Mukundan, A. Shrotri, Q. Ma and J. Beltramini, *ChemCatChem*, 2015, **7**, 781-790.
39 R. Palkovits, K. Tajvidi, A. M. Ruppert and J. Procelewska, *Chem. Commun.*, 2011, **47**, 576-578.
40 F. Lefebvre, F. X. Liu-Cai and A. Auroux, *J. Mater. Chem.*, 1994, **4**, 125-131.
41 T. Okuhara, T. Nishimura, H. Watanabe and M. Misono, *J. Mol. Catal.*, 1992, **74**, 247-256.
42 M. A. Harmer and Q. Sun, *Appl. Catal. A*, 2001, **221**, 45-62.
43 E. Medina, R. Bringué, J. Tejero, M. Iborra and C. Fité, *Appl. Catal. A*, 2010, **374**, 41-47.
44 V. V. Ordomsky, J. van der Schaaf, J. C. Schouten and T. A. Nijhuis, *J. Catal.*, 2012, **287**, 68-75.
45 J. S. Kruger, V. Choudhary, V. Nikolakis and D. G. Vlachos, *ACS Catal.*, 2013, **3**, 1279-1291.
46 B. F. M. Kuster, *Starch - Stärke*, 1990, **42**, 314-321.
47 S. De, S. Dutta and B. Saha, *Green Chem.*, 2011, **13**, 2859-2868.
48 S. J. Dee and A. T. Bell, *ChemSusChem*, 2011, **4**, 1166-1173.
49 M. Dourson, J. Reichard, P. Nance, H. Burleigh-Flayer, A. Parker, M. Vincent and E. E. McConnell, *Regul. Toxicol. Pharm.*, 2014, **68**, 387-401.
50 Y. Yang, C. Hu and M. M. Abu-Omar, *Journal of Molecular Catalysis A: Chemical*, 2013, **376**, 98-102.
51 G. Yang, C. Wang, G. Lyu, L. A. Lucia and J. Chen, *BioResources*, 2015, **10**, 5863-5875.
52 W. Schwald and O. Bobleter, *J. Carbohydr. Chem.*, 1989, **8**, 565-578.
53 P. F. Siril, H. E. Cross and D. R. Brown, *J. Mol. Catal. A: Chem.*, 2008, **279**, 63-68.